

Position Tracking and Flaw Visualization in Conductive Materials

RAFIC BACHNAK

Texas A&M International University
Laredo, Texas 78041, USA
rbachnak@tamiu.edu

SCOTT A. KING

Texas A&M University-Corpus Christi
Corpus Christi, Texas 78412, USA
Scott.king@tamucc.edu

Abstract: - The Eddy current technique has been successfully used in a variety of non-destructive evaluation applications including detection of cracks, measurements of material thickness, examining metal thinning, measurements of coating thickness, identification of materials, and detection of corrosion. This paper shows how positional and eddy-current data are combined to produce a C-scan of flaws in conductive materials. A system that consists of an eddy current probe, a position tracking mechanism, and basic data visualization capability was built and tested. Test results of the prototype are presented and briefly discussed. Improving the accuracy of the measurements using a three-mouse position sensing device is described.

Key-Words: - Position tracking, non-destructive evaluation, eddy current, visualization

1 Introduction

Nondestructive Testing (NDT) plays an important role in ensuring that components and systems are free of defects that compromise their functionality. NDT testing techniques, for example, are used to locate flaws that might otherwise cause major catastrophic events such as plane crashes, train accidents, and plant explosions. Nondestructive Evaluation (NDE) refers to the process of locating defects and providing some measurements about the defect such as length, depth, and orientation. While there are several NDT methods, the three widely used techniques for materials testing and evaluation are radiography, ultrasonic, and eddy-current. The eddy current method relies on the principle of magnetic induction using an alternating current as illustrated in Fig. 1. When an alternating current is supplied to the eddy current transducer (primary coil), an alternating magnetic field is produced. This magnetic field induces a current in a second coil (pick up coil) in close proximity to it. Eddy currents flow in circles in the material being tested. An interruption in the flow of eddy currents may be directly linked to imperfections, such as cracks. In general, an eddy current system is used to inspect a relatively small area and the probe must be selected after a good understanding of the type of defect to be detected. Eddy current data can be collected manually or using automated scanning systems, where the probe moves at a constant speed. Automated systems have the advantage of minimizing changes in lift-off and accurate indexing due to the constant speed. Lift-off refers to the separation between the probe and the surface of the material being tested.

The depth of the eddy currents is a function of the frequency of the excitation current and both the electrical conductivity and the magnetic permeability of the material. The depth of penetration decreases with increasing frequency and increasing conductivity and magnetic permeability.

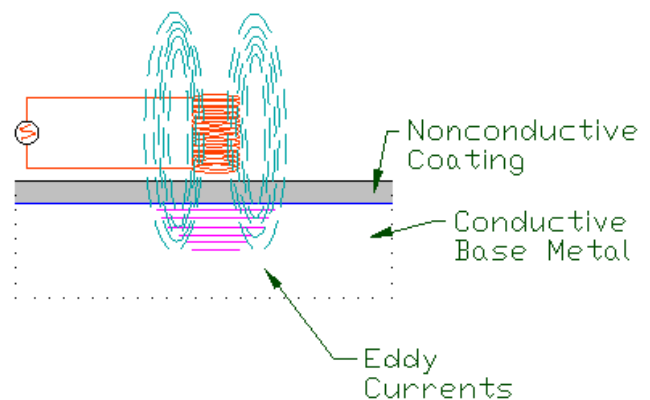


Fig. 1 Eddy-current in conductive materials

Eddy current density decreases exponentially with depth as shown in Fig. 2. The depth at which eddy current density has decreased to $1/e$, or about 37% of the surface density, is called the standard depth of penetration (δ) and is given by the following equation.

$$\delta = \frac{1}{\sqrt{\pi f \mu \sigma}} \quad (1)$$

Where

δ = Standard Depth of Penetration (mm)

π = 3.14159

f = Test Frequency (Hz)

μ = Magnetic Permeability (H/mm)

σ = Electrical Conductivity (% IACS)

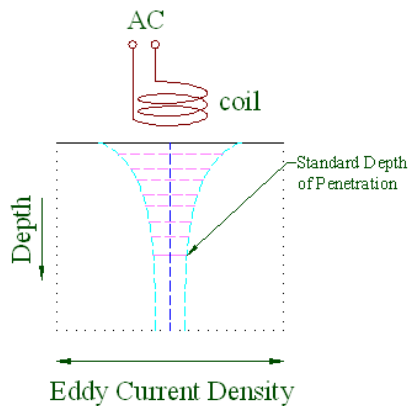


Figure 2. Eddy current density in function depth

μ is equal to $\mu_r \mu_0$. μ_0 , the permeability of free space, is equal to $4\pi \times 10^{-7}$ N/A. At two standard depths of penetration (2δ), the eddy current density decreases to $1/e$ squared or 13.5% of the surface density. At three depths (3δ), the eddy current density decreases to only 5% of the surface density. The minimum thickness for a desired standard depth of penetration may be given by [15]:

$$\text{Minimum thickness} = 2.6 * \delta \quad (2)$$

where δ is given by

$$\delta = 26 * (f \sigma)^{-1/2} \quad (3)$$

This equation, compared to equation 1, assumes an aluminum material with a relative permeability μ_r of 1. Using equations 2 and 3, then the optimum frequency for a desired standard depth of penetration in aluminum is given by:

$$f = 676 * \delta^{-2} * \sigma^{-1} \quad (4)$$

For surface cracks, the frequency should be as high as possible for increased resolution. For subsurface cracks, lower frequencies are required. Reference standards of similar material and thickness to the component being inspected and with representative defects should be available. These standards typically consist of three or four aluminum plates that are fastened together, with artificially induced cracks located in the different layers.

The eddy current method has been used in several industries, including space [1-3] and chemical processing [4, 5]. Some specific applications include detection of cracks [6-10], measurements of material thickness [11], determining metal thinning due to corrosion [12], measurements of coating thickness [13], conversion coating [14], determining electrical conductivity [15], heat damage detection [4], and detection of corrosion in heat exchanger tubes [5]. This paper describes an inspection system that combines positional and eddy-current data to produce a visual representation of materials being tested and discusses recent efforts to improve the accuracy of the positional data [16]. The system consists of an eddy current probe, a position tracking mechanism, and basic data visualization capability.

2 Position Tracking

Two devices were evaluated for the purpose of detecting positional data. The first device, ShapeTape by Measurand Inc., is an array of fiber optic bend and twist sensors attached to a thin flexible substrate. A ShapeTape as used in the laboratory is shown in Fig. 3 (a) and (b). Light intensity is used to calculate six-degree-of-freedom Cartesian data (x, y, z, roll, pitch, and yaw) at closely-spaced intervals along the tape. Cartesian data is found by an integration of angles between small straight segments used to model the continuous curves of the flexure. Sample test results are shown in Table 1, where the positional error can exceed 6%. Even though only information from sensors at the tip is required, the whole tape is needed for acquiring data. This prevents wireless transmission at the tip location and makes the insertion tube bulky. As a result, the device was not selected for the proposed system.

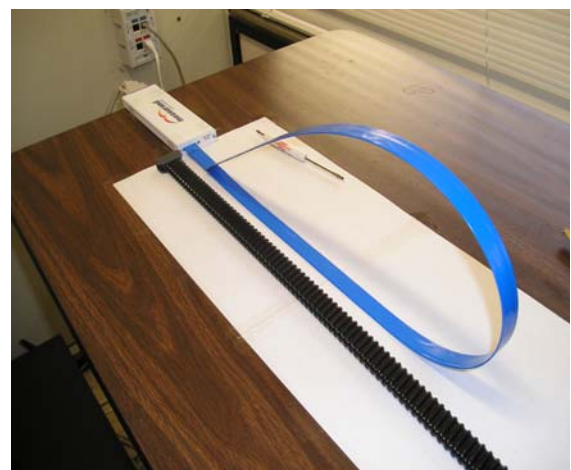


Fig. 3 (a) ShapeTape testing set-up

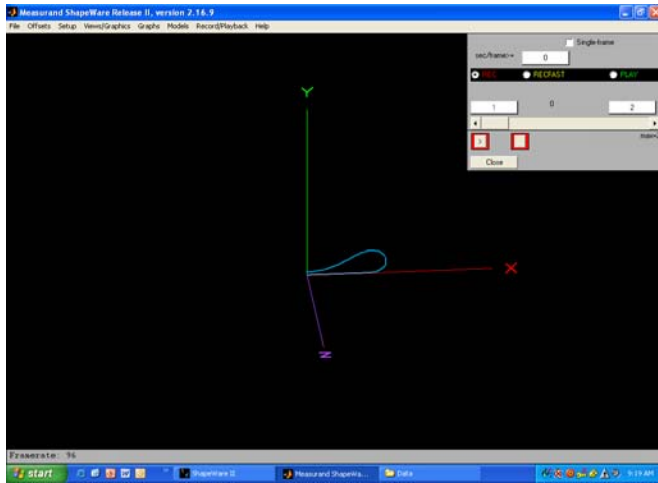


Fig. 3 (b) ShapeTape sample display

Table 1. ShapeTape sample test results

Exp #	Manual Measurements			Shape Tape Measurements			% Error
	X ₁	Y ₁	Z ₁	X ₂	Y ₂	Z ₂	
1	0	0	0	23	-29	-23	4.5
2	300	10	100	305	15	86	1.6
3	300	10	-100	320	-19	-106	3.7
4	957	0	70	955	57	43	6.6
5	957	0	-70	956	38	-49	4.5

The positional error (PE) was computed as follows:

$$PE = \text{SQRT}[(X_1 - X_2)^2 + (Y_1 - Y_2)^2 + (Z_1 - Z_2)^2]$$

The second device is a laser computer mouse. Initially we used the MX-1000 by Logitech. This model was chosen for its characteristics and because we could purchase the main components independently. The mouse consists of the following three major components: (a) A low power laser with a fault protection circuit, (b) A lens that focuses the light emitted from the laser to illuminate the surface seen by the imaging chip, and (c) An imaging chip that contains a digital signal processor and an image acquisition system. The laser mouse was tested using a milling machine and AutoCAD. The milling machine precisely controls the physical distances that the device moves while AutoCAD records the movements produced by the mouse and accurately dimensions them. A gradient

pattern, as shown in Fig. 4, was created to provide an optimal surface for the laser mouse to determine its movements.

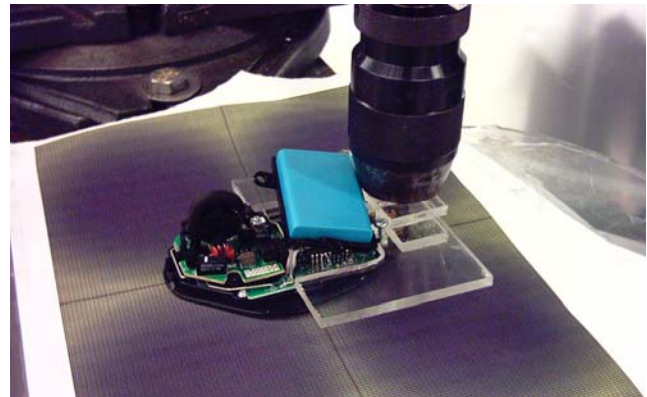


Fig. 4 Gradient pattern used in testing mouse

This surface is used to minimize surface generated error so that only the error generated from the Charged Coupled Device (CCD) is recorded. It is also used to determine a scaling factor to adjust the scale within AutoCAD for the tests. The testing surface was raised to the device as close as possible. The sensing device must be in a perpendicular position in relation to the bottom of the test piece. AutoCAD was set for sketching using increments of 0.001. The sketch feature draws a series of attached straight lines in relation to the movement of the mouse. The increment size determines the length of the attached lines. The larger the increment sizes, the more jagged the curves will appear. The “pendown” command was used to cause AutoCAD to record the mouse movements. Scanning a square shape by moving 10 mm in each direction was used to produce a 10x10 mm square. Once the square is completely drawn, it is scaled. This is needed as the sketch feature in AutoCAD draws the same sketch size in relation to screen size regardless of how far out you are zoomed. A scale factor is determined through the use of the average distance for all sides of the entire test performed on the gradient pattern. Recorded data is entered into Excel and the average for each direction is calculated as well as the standard deviation. Average % error varied between 1.5% and 7.6%. The laser mouse outperformed the shape tape and was chosen for our prototype.

It is important to note that the mouse works by shining a light source, in this case a laser, at an angle onto the surface and using an imaging sensor to collect the bounced light. Using motion detection algorithms, relative motion of the mouse is determined. However, this motion is relative to the sensor chip. If the sensor chip is rotated, then the relative motion vectors also rotate. With a single mouse there is no way to detect this

rotation.

3 Development of a Prototype

Fig. 5 shows the hardware used in the prototype. The major components are an eddy current system, the Nortec 2000D+, an eddy current probe, a Copperhead laser mouse by Razer, and a data acquisition device, USB-1208FS. The USB-1208FS interfaces the Nortec 2000D+ with the laptop.



Fig. 5 Prototype major components

3.1 Acquiring Positional Data

To be able to produce a visualization of defects, positional data is combined with eddy current data to produce a C-scan of the examined material. To acquire positional data, an MX-1000 laser mouse was originally employed. This mouse has a 800DPI resolution and an update rate of 250Hz. To be able to detect a feature that is .050", then a sample is needed every .025". That means the probe can travel no faster than $.025'' * 250/s = 6.25''/s$. To scan the target surface of 12"x12" it would take about 1.92s for each scan. To detect features down to .050" in size, a scan every, .025" would be required, or 480 scans, which would take a minimum of 15 1/2 minutes. In order to reduce the time taken to scan a panel we chose to use the Copperhead from Razer due to its higher resolution and frequency. The Copperhead images at 4000 DPI and has a refresh rate of 1000Hz. This increased resolution and 4x update rate, decreases both the error and the scan time. The system uses a cross-platform API, called ManyMouse, that abstracts using multiple mice into a single small library [17].

3.2 Digitizing Data from the Probe

The Nortec 2000D+ eddy current system, the device

used in the prototype, operates at 6000 Hz. Along with displaying the sensor information on its built-in screen, the Nortec 2000D+ also has two analog outputs that correspond to the horizontal and vertical positions of the cursor on the screen. These outputs must be digitized before they can be used [18]. For testing purposes, a Measurement Computing USB-1208FS digitizer was used. This 12-bit digitizer has a USB interface which allows easy interface with the laptop. It also allows the display of information as it is captured on the laptop's screen.

The USB-1208FS digitizer is not designed to be a low-latency digitizer. That is, it cannot digitize samples at 6000 Hz. Since two signals have to be sampled, its effective capture rate is halved. However, since the positional data is only updated at 1000 Hz, the digitizer only needs a comparable speed. In our prototype environment, the USB-1208FS achieves ~150 Hz, which is adequate for testing purposes. The USB-1208FS can be put in continuous scan mode, or in single capture mode. In continuous scan mode, it captures multiple samples and returns them. In this mode it is capable of capturing at much higher rates, on the order of 100 KHz. However, in order to use the mode, a complex multithreading system with a high-precision clock would be required. It is also possible to use a more expensive and faster digitizer.

The software library that comes with the USB-1208FS is binary-only, and only works on Windows XP. Currently, a Linux driver, written by Warren Jasper of NC State, is used [19]. This is the only piece of the system that is not platform independent. However, it is only an initialization routine and a call to collect a sample that needs to be updated.

3.3. Testing the Prototype

The prototype was tested using the aluminum plate shown in Fig. 6. The plate is approximately .250" thick and has 8 grooves 1" apart. The grooves are rounded at the bottom and are .015" thick. The depths of the grooves are: .005", .010", .040", .060", .080", .100", .100", and .200". Since the grooves are rounded, the first groove isn't as thick as the others, but about .010" thick. Protective tape was applied to the plate to keep it from getting scratched by the probes. Fig. 7 shows a visualization of the front side of this test plate using a pencil probe operating at 300 KHz. Since the mouse and probe were not held a fixed distance from each other, and since the mouse was held by hand there are positional errors. However, the results demonstrate the feasibility of the system for detecting front-side cracks and shows that visualization with this approach is possible.

Visualizations were developed as C++ programs

written for Linux with OpenGL for performing the graphics [20]. OpenGL is a cross-platform graphics library. All of the code for this project, except for the Linux-only USB-1208FS Linux driver, uses cross-platform libraries that have source code available. Even though C++ is used, there are few advanced features used, and with a small effort the entire project can be recompiled in C.

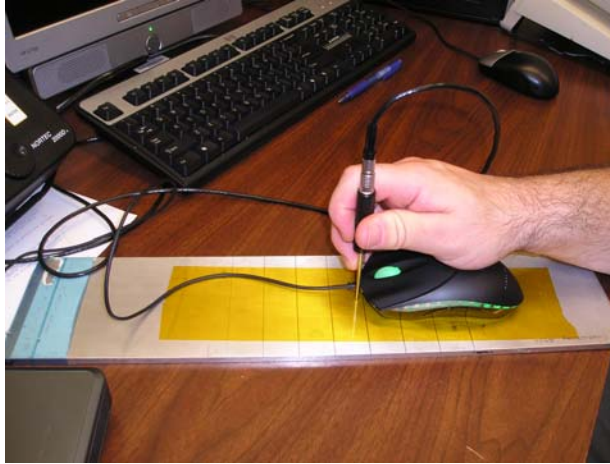


Fig. 6 Scanning an aluminum plate

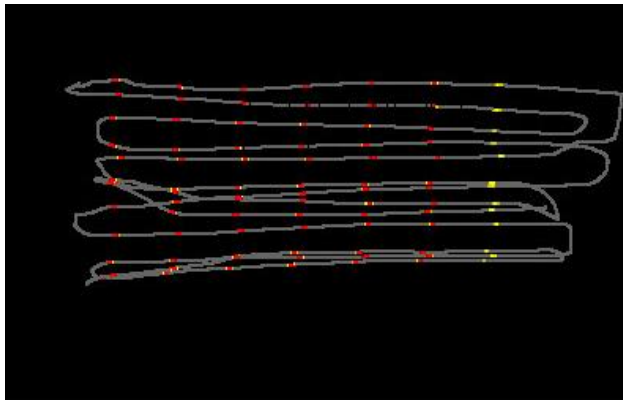


Fig. 7 Visualization of plate shown in Fig. 5

The prototype was also tested for a backside inspection of the plate. The backside inspection was completed with a 100 Hz – 20 KHz frequency probe. Since the probe is much thicker than a pencil probe (0.6”), it responds to the same crack over a larger distance. This causes much larger lines in the visualization. Fig. 8 shows results of a sample test with an operational frequency of 300 Hz.

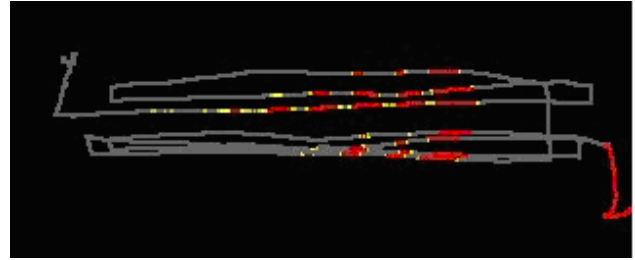


Figure 8. Visualization of a backside inspection

4 Three-Mouse System

A jig that holds three mice and an eddy current probe, as shown in Fig. 9, was built and has been used to test and develop an algorithm to determine absolute position. Each mouse is situated such that the direction “up” on the mouse points toward the center of the jig, and each mouse is separated from the other mice by the same distance. Each mouse sends the computer updates on its “position” as relative motion; that is, a mouse sends two numbers that describe to the computer how far in x and how far in y the mouse has moved.



Fig 9. Three-mouse positioning jig

4.1 Determining Mouse Precision

The Razer Copperhead high-precision laser mouse is used to build the positioning system. The manufacturer advertises the mouse to have a precision of 2000 counts per inch with an update rate of 1000 Hz. In order to use the mouse for position tracking the exact resolution must be known since we are determining absolute position and not just whether or not motion has occurred.

Several experiments were designed to determine how accurately and consistently the mouse registers movements in a real world plane. A milling machine, shown in Figure 10, capable of moving the mouse in

very precise distances across our testing surface was used. In order to use the milling machine, a hole was drilled in the top of the mouse case through which a hexagonal rod was attached with a screw. The rod was heated with a soldering iron to melt the plastic into place around the rod, countersinking the screw. This allowed the mouse to be attached to the milling machine.



Figure 10. Milling machine test setup.

4.1.1 Experiment 1

The first experiment was designed to determine how direction and angle affected precision and accuracy. The mouse was moved left, right, up, down, and at a 45° angle for 1 inch using the milling machine. The mouse reported numerous movements during the test and the total count was added up. Table 2 shows the results from the ten trials conducted.

Table 2. Results from experiment 1.

	left	right	Up	down	45°
avg	2260	2340	2298	2264	2318.0
σ	7.63	7.70	4.66	6.55	22.027

4.1.2 Experiment 2

The next experiment was designed to see if the mouse was sensitive to velocity. For this experiment, the mouse was mounted and aligned as closely as possible to a straight up and down orientation. 20 tests of 8 inches in length as fast as the automatic milling motor would go were run. At this speed, it took about 10 to 12 seconds

to travel the full 8 inches. This was followed by ten more tests only as slowly as possible. At this speed, it took about ten minutes per run of 8 inches. The average number of pixels traveled in each direction was recorded and the average total distance in pixels was calculated for both methods. There does not appear to be much difference between the two speeds. However speed cannot be higher using the milling machine. The results of this experiment were similar to experiment 1 and are shown in Table 3.

Table 3. Results from experiment 2.

	fast	slow
Avg. CPI	2261.09	2257.90
σ	6.64	6.73

4.1.3 Experiment 3

The object of this experiment was to get data for relatively high speeds of mouse motion. This test was run manually. To be as accurate as possible, two boards were clamped parallel onto a table such that the space between was 10 inches plus the width of the mouse. A ruler was clamped perpendicularly to serve as a guide. By beginning at one end of the ruler, pressed against the board, and moving along the ruler to the other board, results were recorded. The setup is shown in Fig. 11. This is really an extension of the previous experiment, just done manually. This is also a better indicator of system performance if the final system will be used manually.

The mouse was moved the entire 10 inches in the space of about a second. Once the data had been recorded for 30 trials at the highest mouse resolution and hertz, the experiment was repeated with the lowest settings for another 30 trials. We captured the number of pixels in each direction and calculated the total distance assuming that the mouse's orientation remained constant. For this experiment, the average resolution over the 30 trials was 2240.7cpi with a standard deviation of 18.11.

4.1.4 Experiment 4

During slow movement, the position system was seeing large error in the rotation calculation. This seems to be due to the mouse being more sensitive when moved equally in both mouse axes instead of parallel to one. Based on the results of the first experiment and the error the system was encountering, we conducted an

experiment where the mouse was moved 8 inches with the mouse aligned at differing angles against the movement. The experiment was run at 15 degree intervals. Due to the length of time it takes to do each trial and with 7 different angles, we originally only performed five trials. The results surprised us so we conducted five more trials. The results we not as consistent as we would like so we conducted another set of 20 trials. The results of all 30 trials are shown in Fig. 12. The standard deviation of the value for the counts per inch ranged from 10 to 35. When the motion is along a principle axis, the standard deviation was much lower with the high standard deviations at 15 and 75 degrees. Our conclusion is that the imaging chip used does not have square pixels and thus has differing resolutions along each axis.



Fig. 11. Setup for experiment 3.

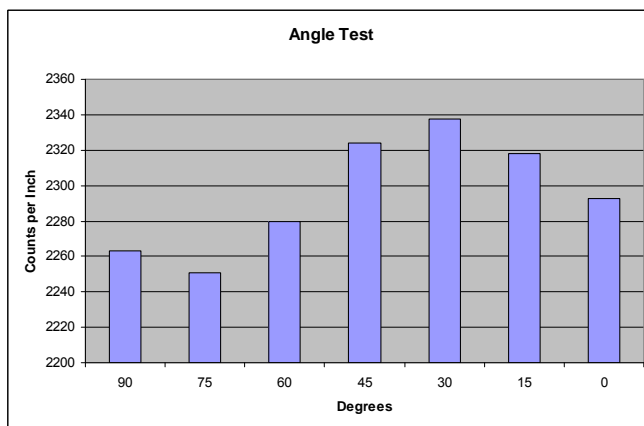


Fig. 12 Comparison of counts per inch versus the angle the mouse is moved at.

4.2 Determining Absolute Position

When a mouse motion event is detected, our program reads in values reported by each mouse at that moment. Then, from these readings, we must calculate the translation and rotation of the jig. The linear translation can be found by calculating the mean of the motion vectors of each mouse. The more difficult task consists of determining the rotation of the jig. We are using the method described by Jain [21] to calculate this rotation at each discrete position. The rotation between the absolute initial position (the “zero position”) and the new position is calculated each iteration.

First, the raw data values received from the mice, m_i , are a vector representing how each mouse has recently moved and are in the local coordinate system of each mouse. These motion vectors must then be transformed into a common jig coordinate system P_i . This is accomplished with:

$$P_i = X_i m_i$$

The jig coordinate system is axis-aligned with the first mouse and the origin is in the center of the jig. Two of the mice on the jig are rotated by an angle of 120 degrees, so the transformation X_i consists of a constant rotation, and a constant translation of each mouse’s initial position.

To go from jig coordinates into world coordinates, we first apply the last known rotation of the jig to each motion vector: $P_i' = R P_i$. To get the new jig position in world space all we need to do is add the average of the motion vectors to the old position:

$$T' = T + \frac{P_1' + P_2' + P_3'}{3}$$

Now we need to determine how the jig has rotated, so we can repeat this process. To find the rotation matrix, R , we first translate the final position coordinates’ centroid to the origin, by subtracting the centroid from each point. Then, because the initial position is always centered at $(0, 0)$, we have two sets of points which differ only by a rotation, and possible measurement error.

We treat each point as a ray. Taking the dot product of two corresponding rays gives us the angle between them. This is what we would do if we had only one pair of rays to work with, but with our jig, we have three pairs of rays, with each pair consisting of an “old” and a “new” ray. Suppose we apply some rotation matrix R to each of the new rays to rotate the new rays back to the position of the old rays. We want R to be a “best fit” rotation. If we take the dot product of each old ray with

its corresponding new ray, and sum the results, we can calculate R. The best fit R maximizes:

$$\chi = \sum [p_i \bullet Rq_i]$$

Here, p_i is a vector representing a mouse position from the initial jig position (which is constant in our case), q_i is a vector representing a mouse position in the current jig position, and R is the 2x2 rotation matrix between them. For the rest of these equations, the subscript i will be dropped for readability.

Given

$$\begin{aligned} p &= (x_{old}, y_{old}) \\ q &= (x_{new}, y_{new}) \\ R &= \begin{bmatrix} r_{11} & r_{12} \\ r_{21} & r_{22} \end{bmatrix} \end{aligned}$$

χ can be calculated as:

$$\chi = r_{11}S_{xx} + r_{12}S_{yx} + r_{21}S_{xy} + r_{22}S_{yy}$$

where

$$S_{ab} = \sum a_{new} b_{old}$$

and r_{ij} represents the component of R occupying row i and column j of the rotation matrix.

Here, instead of using an eigenvalue approach as in Jain, we use a few properties of 2x2 matrices of rigid body rotation. We know that for a 2d rigid body rotation matrix:

$$\begin{aligned} r_{11} &= r_{22} \\ r_{12} &= -r_{21} \\ r_{12} &= \pm \sqrt{1 - r_{11}^2} \end{aligned}$$

Substitution gives:

$$\chi = r_{11}(S_{xx} + S_{yy}) \pm \sqrt{1 - r_{11}^2}(S_{yx} - S_{xy})$$

Since we're maximizing χ , and we now have χ as a function of one variable, we simply take the derivative with respect to r_{11} and set it equal to zero:

$$0 = \frac{d\chi}{dr_{11}} = S_{xx} + S_{yy} \pm \frac{r_{11}}{\sqrt{1 - r_{11}^2}}(S_{yx} - S_{xy})$$

Solving this yields:

$$r_{11} = \pm \sqrt{\frac{q^2}{1 + q^2}}$$

where

$$q = \frac{S_{xx} + S_{yy}}{S_{yx} - S_{xy}}$$

So now we have two choices of values for r_{11} and two choices of values for r_{12} . Once these are chosen, r_{21} and r_{22} are determined. All that remains is to calculate χ for all 4 possible sets of values of r_{11} and r_{12} , and choose the pair that gives the highest value for χ , and we have found our rotation matrix R.

5 Fabricating a Test Platform

To test the three-mouse device, a testing platform with dimensions of 18.03125 inches long by 4.125 inches wide by .250 inches thick is needed. As shown in Figure 13, the fabricated platform consists of a testing plate sandwiched between two fiber boards. All three plates were drilled with a .156 in. drill and then a countersink was used for the wood fasteners used for this project. The testing board and the two sections of fiber board were attached using one inch wood fasteners (screws) that were trimmed by grinding the ends to have a flush finish with the mounting board.

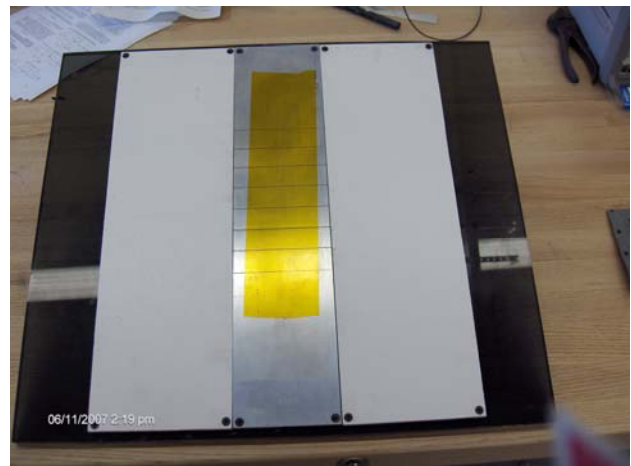


Fig. 13 Three-mouse testing platform

6 Recent Work

We are now working on adding gyroscopes, mounted on the laser mouse device, to add three-dimensional data acquisition capabilities to the system. The approach is to have the mouse maintain its normal 2D function to display translation along a plane, and an additional function provided by the gyroscopes that will provide the angular position of the mouse in relation to the starting point, or origin. The main program works by reading “vectors” created after every predetermined delay. For example, if the time precision in the program is set to 1 ms, then the program will read the distance travelled by the mouse in X and Y after every 1 ms (and therefore creating a vector for that time lapse). The default value for this feature is 1 ms since it is the smallest delay that the program can produce effectively. These vectors are recorded and added to form what seems to appear as a free hand sketch of the mouse trajectory (very tiny lines). Fig. 14 shows the results of an experiment for a 1.5 foot trajectory sketched with 1270 lines.



Fig. 14 1.5 foot trajectory sketched with 1270 lines

A couple of seconds after the user stops moving the mouse, the program will stop and save all the coordinates in a script with a layout “readable” for AutoCAD. These can be examined by the user directly or executed in AutoCAD as a script file and thus a lot easier to read. Judging visually, the program works extremely well and accurate. The program can now run as fast as 1 kHz but can be slowed down to save memory and CPU power.

7 Conclusion

This paper showed how data from an eddy current probe can be combined with positional data from a laser mouse to produce a C-scan of tested material. The prototype consists of an eddy current probe, a position tracking mechanism, and basic data visualization capability.

Improving the accuracy of the system by using a three-mouse positioning device is being explored.

Acknowledgement

This project is partially supported by a grant from NASA-Johnson Space Center.

References:

- [1] R. Smith, G. Hugo, “Transient Eddy-current NDE for Aging Aircraft – Capabilities and Limitations,” Proc 4th Joint DoID/FAA/NASA Conf on Aging Aircraft, May 2000.
- [2] A. Ahmed, J. G. Bakuckas, Jr., C. A. Bigelow, P. W. Tan, J. Awerbuch, A. Lau, and T. Tan, “Initiation and Distribution of Multiple-Site Damage (MSD) in a Fuselage Lap Joint Curved Panel,” Proceedings of the 5th Joint NASA/FAA/DoD Conference on Aging Aircraft, September 10-13, 2001, Kissimmee, FL.
- [3] R. Bachnak and S. King, “Non-Destructive Evaluation and Flaw Visualization Using an Eddy Current Probe,” The Third Int. Conf. on Systems (ICOS 2008), CD-ROM Proceedings, ISBN: 978-0-7695-3105-2, pp.134-139, Cancun, Mexico, April 13-18, 2008.
- [4] A. Birring and G. Marshall, “Eddy Current Testing in the Petrochemical Industry,” Materials Evaluation, November 2003.
- [5] Helle H. Rasmussen, Hans Kristensen, and Leif Jeppesen, “NDT and Heat Exchanger Tubes,” NDT.net October 1998, Vol.3 No.10.
- [6] Y. Wu, C. Hsiao, “Reliability Assessment of Automated Eddy Current System for Turbine Blade,” NDT.net, Vol. 7, No. 11, November 2002.
- [7] S. Burke, “Crack Depth Measurement using Eddy-Current NDE,” 10th Asia-Pacific Conference on Non-Destructive Testing , 17-21 September 2001, Brisbane, Australia.
- [8] D. Moore and F. Spencer, “ Interlayer Crack Detection Results Using Sliding Probe Eddy Current Procedures,” 10th Asia-Pacific Conference on Non-Destructive Testing , 17-21 September 2001, Brisbane, Australia.
- [9] B. Wincheski, J. P. Fulton, S. Nath, M. Namkung, and J. W. Simpson, “Self-Nulling Eddy Current Probe for Surface and Subsurface Flaw Detection,” in Materials Evaluation, Vol. 52/Number 1 (January 1994).
- [10] Ryszard Sikora, Piotr Baniukiewicz, “The Complete Measurement System for Crack,” Proceedings of the VIth International Workshop, Computational Problems of Electrical Engineering, Institute of Theory of Electrical

- Engineering, Zakopane, Poland, September 1-4, 2004
- [11] T.K. O'Brien and D.C. Kunerth, "Pulsed Eddy Current Thickness Measurements of Transuranic Waste Containers," US Dept of Energy, Report number INEL--95/00313; CONF-951091-12, 1995.
- [12] J. Skramstad, R. Smith and David Harrison, "Enhanced detection of deep corrosion using transient eddy currents," Proc. 7th Joint DoD/FAA/NASA Conference on Aging Aircraft, New Orleans, Sept 2003.
- [13] "Measuring Coating Thickness," CMI International Inc., Elk Grove Village, Illinois, <http://www.pfonline.com/articles/pfd0027.html>, accessed on November 7, 2005.
- [14] A. Salem, T. Nayfeh, and C Fox, "Nondestructive Quality Assurance Testing of Chemically Processed Wood," Int. Journal Advanced Manufacturing Technology, Springer-Verlag London Limited, Vol. 26, pp. 1275-1283, January 2005.
- [15] Yaron Danon, Changqing Lee, Chris Mulligan, and Greg Vigilante, "Characterizing Tantalum Sputtered Coatings on Steel by Using Eddy Currents," IEEE TRANSACTIONS ON MAGNETICS, VOL. 40, NO. 4, JULY 2004, pp. 1826-1832.
- [16] R. Bachnak, R. Chakinarapu, M. Garcia, T. Nguen, "Real-Time Acquisition and Display of Data and Video," Proceedings of the 7th Int. Conf. on Signal Processing, Computational Geometry, and Artificial Vision (ISCGAV '07), pp. 233-239, Vouliagmeni, Athens, Greece, August 24-26, 2007
- [17] Manymouse, <http://www.icculus.org/manymouse/>, visited July, 2006
- [18] Operating Manual, MIZ-21B Eddy Current System, Zetec, inc., 2003.
- [19] W. Jasper, "Linux Drivers", <ftp://lx10.tx.ncsu.edu/pub/Linux/drivers/>, visited July, 2006.
- [20] OpenGL, <http://www.opengl.org>, visited July, 2000.
- [21] R. Jain, R Katsuri, B Schunck, *Computer Vision*, McGraw-Hill, New York, 1995.